(Article begins on next page)

ACS Infectious Diseases

Article

1,2,3-Triazolylmethaneboronate: A Structure Activity Relationship Study of a Class of β-Lactamase Inhibitors against *Acinetobacter baumannii* Cephalosporinase

Emilia Caselli, Francesco Fini, Maria Luisa Introvigne, Mattia Stucchi, Magdalena A. Taracila, Erin R. Fish, Kali A. Smolen, Philip N. Rather, Rachel A. Powers, Bradley J. Wallar,* Robert A. Bonomo,* and Fabio Prati*

Cite This: https://dx.doi.org/10.1021/acsinfecdis.0c00254

Read Online

ACCESS | Metrics & More | Article Recommendations | Supporting Information

ABSTRACT: Boronic acid transition state inhibitors (BATSIs) are known reversible covalent inhibitors of serine β-lactamases. The selectivity and high potency of specific BATSIs bearing an amide side chain mimicking the β-lactam's amide side chain are an established and recognized synthetic strategy. Herein, we describe a new class of BATSIs where the amide group is replaced by a bioisostere triazole; these compounds were designed as molecular probes. To this end, a library of 26 α-triazolylmethaneboronic acids was synthesized and tested against the clinically concerning *Acinetobacter*-derived cephalosporinase, ADC-7. In steady state analyses, these compounds demonstrated K_i values ranging from 90 nM to 38 μM ($\pm$10%). Five compounds were crystallized in complex with ADC-7 β-lactamase, and all the crystal structures reveal the triazole is in the putative amide binding site, thus confirming the triazole−amide bioisosterism. The easy synthetic access of these new inhibitors as prototype scaffolds allows the insertion of a wide range of chemical groups able to explore the enzyme binding site and provides insights on the importance of specific residues in recognition and catalysis. The best inhibitor identified, compound **6q** (K_i 90 nM), places a tolyl group near Arg340, making favorable cation−π interactions. Notably, the structure of **7q** does not resemble the natural substrate of the β-lactamase yet displays a pronounced inhibition activity, in addition to lowering the minimum inhibitory concentration (MIC) of ceftazidime against three bacterial strains expressing class C β-lactamases. In summary, these observations validate the α-triazolylboronic acids as a promising template for further inhibitor design.

KEYWORDS: boronic acids, Acinetobacter, amide bioisostere, click chemistry, β-lactamase inhibitors
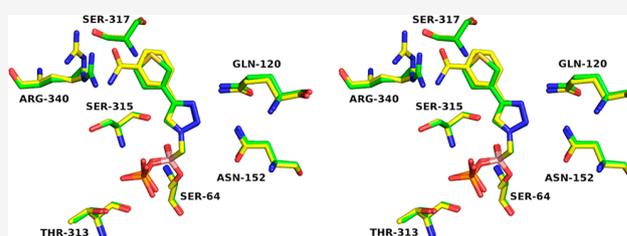
Antimicrobial resistance (AMR) is a major global health threat. Regrettably, this crisis is aggravated by the lack of new therapeutic agents in the current pharmaceutical pipeline. Economic analyses indicate that AMR increases health-care costs, the length of stay in the hospital, morbidity, and mortality.[1] For these reasons, the World Health Organization (WHO) has recently designated AMR as one of the three most important problems facing human health.[2] The WHO Priority List has recently assigned *Acinetobacter baumannii* as a critical priority pathogen due to the high prevalence of cephalosporin and carbapenem resistance and its ability to survive in adverse environmental conditions, making it one of the most threatening nosocomial pathogens.[3]

Common AMR mechanisms found in *Acinetobacter* spp. include modification of the enzymes that the antibiotic targets, decreased permeability of the outer membrane, efflux pumps, and the production of enzymes that attack and inactivate antibiotics (β-lactamases).[3,4] Current antimicrobials used in the clinic to treat infections caused by multidrug resistant (MDR) or extreme drug resistant (XDR) *A. baumannii* are siderophore containing β-lactams (cefiderocol), polymyxins, tigecycline, and aminoglycosides. All these drugs display uncertain clinical efficacy, a high level of toxicity, and mounting resistance.[4] The urgent need for new drugs active against this pathogen has recently accelerated drug development, and new therapeutic options are under study.

The attractiveness of identifying β-lactamase inhibitors effective against *A. baumannii* relies upon the β-lactam's intrinsic mechanism of action. The use of combination therapy, where a β-lactam antibiotic is combined with a β-lactamase inhibitor, is a time-honored and extremely effective approach to overcome resistance. Three new β-lactam/β-lactamase inhibitor combinations recently entered the market, namely, the diazabicyclooc-

A

tane avibactam with ceftazidime (Avycaz),[5] relebactam with imipenem/cilistatin (Recarbrio), and the boronic acid vaborbactam with Meropenem (Vabomere).[6] While these combinations prove to be useful in the treatment of infections caused by carbapenem resistant *Enterobacteriacae* and multi drug-resistant (MDR) *P. aeruginosa*, they are not uniformly active against *A. baumannii*.[7] *A. baumannii* possesses many clinically diverse β-lactamases from all four classes; the most significant portion of β-lactam resistance in *A. baumannii* is expressed by class C *Acinetobacter*-derived cephalosporinases (ADCs), chromosomally encoded β-lactamases responsible for resistance to advanced generation cephalosporins.

In previous work, we systematically evaluated the activity of a series of boronic acids against ADC-7, a representative class C enzyme found in *A. baumannii*.[8] Boronic acid transition state inhibitors (BATSIs) are known reversible covalent inhibitors of β-lactamases, due to the electrophilic character of the boronic moiety, which upon attack of the nucleophilic serine residue, forms a tetrahedral adduct with the enzyme.[9] Selectivity and high potency of specific BATSIs toward β-lactamases were identified in several studies, by means of changing the substituents on the carbon atom attached to the boron. The first scaffold (**A**) that proved active against ADC-7 was a chiral α-acylaminoalkaneboronate (Figure 1),[10] where the α-carbon

Figure 1. BATSI scaffolds for ADC-7 inhibitors.

atom was substituted by a canonical R$_1$ amide side chain in position C6/C7, typical of penicillins/cephalosporins, and a R$_2$ group bearing a carboxylate, which is always present in position C3/C4 of the same β-lactam antibiotics. To this scaffold belongs compound SM23, the best inhibitor of this series with a K_i of 21 nM for ADC-7.[8]

A second scaffold (**B**) was subsequently designed that replaced the amide group with a sulfonamide.[11] With this class of derivatives, the natural substrate mimetics of scaffold **A** (both the R$_1$ and R$_2$ inspired by the β-lactam structures) were advanced into a series of compounds that could better "fit" into the enzyme active site. Compound **CR192** from series **B** demonstrated a K_i of 0.45 nM, proving one of the most potent inhibitors of ADC-7 ever designed. Finally, in series **C**, the amide/sulfonamide was replaced by a triazole ring. Triazoles are nonclassical amide bioisosteres[12] and share with the amide a wide range of properties such as planarity, size, dipole moment, and hydrogen bonding capabilities. Indeed, even though **S06017** is a less potent inhibitor (K_i = 6.1 μM) compared to the achiral sulfonamide **CR192**, the structural information from the X-ray crystal structure of the enzyme−inhibitor complex suggested that the triazole maintained two of the canonical interactions in the amide binding site, thus behaving as a good amide bioisostere.[11]

Encouraged by the bioisosterism and the easy synthetic access of α-triazolylboronic acids **C**, we chose to explore the potential of this particular scaffold in the present analysis, specifically 1,2,3-triazoles 1,4-disubstituted that are easily accessible through 1−3-dipolar Cu-catalyzed azide−alkyne cycloaddition (CuAAC).[13] Our goal was to use these compounds as molecular probes to elucidate structure activity relationships, SAR. The Cu-based process employs click chemistry, which proceeds in mild conditions, using inexpensive reagents, with high efficiency and simple product isolation. Furthermore, we have already demonstrated the tolerance of boronic esters with CuAAC.[14−17] In this paper, 26 compounds were synthesized and characterized via kinetic analysis and microbiological assays. The extraordinary inhibitory activity against ADC-7 was determined (K_i values spanning from 90 nM to 33 μM) and compared with vaborbactam binding affinity of 0.72 μM (IC$_{50}$ 14.6 μM). Additionally, the X-ray crystal structures of ADC-7 in complex with 5 of these compounds were determined to resolutions ranging from 1.74 to 2.04 Å. Despite being different from the amide, we hypothesized that the triazole would maintain significant potency and selectivity while allowing for easy and straightforward access to a wide variety of derivatives.

RESULTS

Design. The α-triazolylmethaneboronic acid **S06017** (Figure 1), described in a previous publication,[10] displayed a lower binding affinity to ADC-7 (K_i = 6.1 μM) compared to α-sulfonamido and α-acylamidomethane boronic acids. However, the crystal structure of the ADC-7/**S06017** complex showed that the triazole maintained two of the three canonical interactions in the amide binding site, with two nitrogen atoms interacting with Gln120 and Asn152, suggesting that this heterocycle could behave as a good amide bioisostere. Furthermore, the triazolylmethaneboronic acid scaffold was synthetically accessible and allowed for the introduction of different groups at position 4 of the triazole (Scheme 1). For

Scheme 1. Synthesis of α-Triazolylmethaneboronate 6a−q[a]

[a](i) NaN$_3$, CH$_3$CN, 85 °C; (ii) (+)-pinanediol, SiO$_2$, H$_2$O$_2$, overnight; (iii) a−q, CuSO$_4$, Na ascorbate, t-BuOH/H$_2$O, 2 h, 60 °C; (iv) isobutylboronic acid, HCl, acetonitrile, n-hexane, r.t.

these reasons, our goals in this study were to validate whether the α-triazolylmethaneboronic acid group (i) is a good scaffold for ADC-7 inhibition; (ii) serves as a template for new ADC-7 BATSIs capable of restoring antibiotic activity.

To these ends, we strategically designed four series of α-triazolylmethaneboronic acids (Table 1). In Series **I**, five

Table 1

Series I	Series II	Series III	Series IV
6a R = -H **6b** R = 3-CH$_3$ **6c** R = 3-SO$_2$NH$_2$ **6d** R = 3-CO$_2$H **6e** R = 3-CONH$_2$	**6f** R = (thiophene) **6g** R = (pyridine) **6h** R = (pyrazine)	**6i** R = -H **6j** R = 3-Cl **6k** R = 4-OCH$_3$ **6l** R = 3-NAc	**6m** R = ClH$_3$N$^+$ **6n** R = F$_3$C-C(O)NH **6o** R = PhNH-C(O) **6p** R = (tolyl)C(O)NH **6q** R = (tolyl)SO$_2$NH

compounds (**6a**–**e**) contain a phenyl ring directly bound to the triazole with a substituent on the aromatic moiety. Series **II** consists of three triazoles (**6f**–**h**) bearing electron rich and electron poor heterocyclic rings replacing the phenyl, whereas Series **III** (compounds **6i**–**l**) and **IV** (compounds **6m**–**q**) introduce a phenyloxymethyl substituent or a substituted aminomethyl bridge on the triazole in order to confer more flexibility to the structures. The substituents for each series are represented in Table 1.

Synthesis. The synthesis of α-triazolylmethaneboronate was successfully performed as depicted in Scheme 1. The 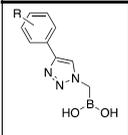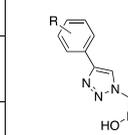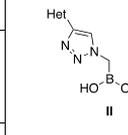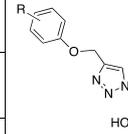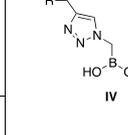commercially available bromomethanetrifluoroborate **1** was reacted with sodium azide in acetonitrile at 85 °C to afford the azidomethanetrifluoroborate **2** in 90% yield.

Conversion of the organotrifluoroborate **2** into the (+)-pinanediol α-azidomethaneboronate **3** was performed in degassed water in the presence of silica gel (1.5 equiv) and a stoichiometric amount of (+)-pinanediol (90% yield). Compound **3** is one of the partners of CuAAC; the acetylene counterparts **4a**–**q** were conveniently purchased or synthesized following literature procedures (see the Methods). The cyclization reactions were carried out as described.[14] The expected 1,4-disubstituted triazoles **5a**–**q**, differently substituted at the R$_1$ group (see Table 1), were easily isolated by extraction and used as such for the next step. Final deprotection of (+)-pinanediol ester **5a**–**q** was accomplished by transesterification with isobutylboronic acid (0.95 equiv) and HCl 3 M (3 equiv) in a biphasic system of acetonitrile/*n*-hexane, allowing one to obtain final boronic acids **6a**–**q**.

Inhibition Kinetics and Antibiotic Susceptibility (Minimum Inhibitory Concentrations, MICs). The binding affinities (K_i) for each of the BATSIs with ADC-7 were determined using competition kinetics with nitrocefin (NCF) used as chromophore substrate. The K_i values (average data from 3 experiments) for all BATSIs, corrected for the NCF affinity (K_m 20 μM), are reported in Table 2.

Table 2. Binding Affinities (K_i) of Compounds 6a–q and Their Contribution to Ceftazidime (CAZ) Susceptibility (MIC)[a]

| Compound	Structure	R	K_i (μM) ADC-7	*E. coli* DH10B *bla*$_{ADC-7}$ MIC CAZ = 16 μg/mL
6a	**I**	-H	0.60 ± 0.04	2
6b		3-CH$_3$	0.49 ± 0.05	4
6c		3-SO$_2$NH$_2$	1.61 ± 0.2	4
6d		3-CO$_2$H	0.90 ± 0.12	2
6e		3-CONH$_2$	0.20 ± 0.03	2
6f	**II**	(thiophene)	1.0 ± 0.2	8
6g		(pyridine)	1.6 ± 0.2	4
6h		(pyrazine)	5.32 ± 0.6	4
6i	**III**	-H	2.84 ± 0.3	8
6j		3-Cl	0.98 ± 0.1	4
6k		4-OCH$_3$	1.54 ± 0.2	4
6l		3-NHAc	1.52 ± 0.2	8
6m	**IV**	ClH$_3$N$^+$	8.69 ± 1	8
6n		F$_3$C-C(O)NH	14.54 ± 2	8
6o		PhNH	3.38 ± 0.4	8
6p		(tolyl)C(O)NH	33.8 ± 4	8
6q		(tolyl)SO$_2$NH	0.09 ± 0.01	2

[a]In contrast, the vaborbactam affinity for ADC-7 is 0.72 ± 0.1μM.

All compounds show inhibition of ADC-7 β-lactamase in the low micromolar range. Compounds from Series **I**, with an aromatic phenyl ring directly bound to the triazole, exhibit K_i

values spanning from 0.2 μM (compound **6e**) to 1.6 μM (compound **6c**). When the aromatic moiety is a heterocycle (Series **II**) or a substituted benzyloxy group (Series **III**), inhibition remains in the low micromolar range, with the thiophene substituent (**6f**) being the best from Series **II** (K_i 1.0 μM) and the 3-chlorophenyl (**6j**), from Series **III** (K_i 0.98 μM). Compounds from Series **IV** (**6m−q**) show the most surprising results, suggesting that the addition of moieties to the triazole to increase flexibility is not always beneficial: activity varies from 33.8 μM for compound **6p** having an amide as a bridge between the triazole and the phenyl ring down to as low as 90 nM for **6q**, which replaces the amide of **6p** with a sulfonamide. This 300-fold difference in activity suggested a possible second round of inhibitor structure refinement. Nevertheless, we wanted to confirm **6q** as the best lead compound using a microbiological profile as well.

The inhibition constant (K_i) values and MIC data (Table 2) for compounds **6a−q** are plotted in Chart 1. Data show a good

Chart 1. Correlation between Synergistic Activity of BATSIs in Combination with CAZ (MICs) against *E. coli* Expressing *bla*$_{ADC-7}$ and Their Binding Affinity for Purified ADC-7 Enzyme (K_i)
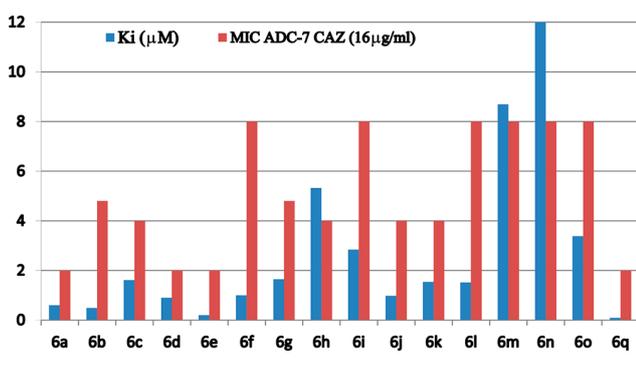
agreement between kinetic and antimicrobial activity: the lower the MIC, the higher is the affinity of the compound. Compound **6q** proved to be the best compound under both kinetic and microbiological profiles.

To further improve the structure of **6q**, we designed another series of triazolyl BATSIs (Series **V**, Figure 2). Nine additional
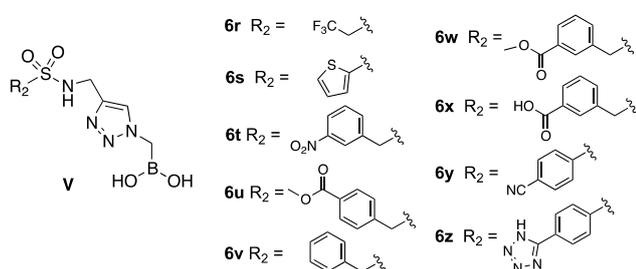

Figure 2. General structure and substituents in Series **V**.

compounds **6r−z** were synthesized with the replacement of the tolyl group of **6q** with a trifluoroethyl (**6r**), a thiophene (**6s**), five different benzyl groups (**6t−x**)m and two *p*-substituted phenyl groups (**6y, 6z**).

Synthesis of compounds **6r−z** followed the same synthetic Scheme 1 (see Methods for detailed description), and their affinity toward ADC-7 (K_i's) and the enhanced activity with the

antibiotic ceftazidime (CAZ) or cefepime (FEP) (MICs) are summarized in Table 3.

Table 3. Binding Affinities (K_i Values) of Series V BATSI Compounds against ADC-7 Enzyme and MIC Values (μg/mL) of CAZ or FEP in Combination with 4 μg/mL of Series V BATSIs

comp	K_i [μM] ADC-7	*E. coli*, DH10B *bla*$_{ADC-7}$	*E. coli*, DH10B *bla*$_{CMY-2}$	*P. aer.* 18SH *bla*$_{PDC}$	*E. coli*, DH10B *bla*$_{CTX-M-9}$
CAZ		16	128	64	
FEP					8
6q	0.09 ± 0.01	2	16	32	1
6r	1.46 ± 0.2	4	32	32	4
6s	0.31 ± 0.04	2	8	64	2
6t	1.02 ± 0.1	2	32	64	4
6u	0.39 ± 0.3	2	64	64	8
6v	0.77 ± 0.08	2	32	64	4
6x	0.31 ± 0.02	2	32	64	2
6w	0.70 ± 0.08	2	32	32	4
6y	0.84 ± 0.07	2	32	64	4
6z	0.21 ± 0.03	2	64	64	4

All compounds from Series **V** present nanomolar (K_i^{6q} 90 nM) to low micromolar (K_i^{6r} 1.46 μM) inhibitory activity against ADC-7 β-lactamase. To assess the capability of these compounds to restore β-lactam susceptibility, broth micro-dilution MICs were performed against three bacterial strains expressing class C β-lactamases and one expressing a class A β-lactamase. The microdilution MICs were performed in 200 μL wells, with BATSI concentrations maintained at 4 μg/mL. The antibiotic partner for class C β-lactamase strains (*E. coli* DH10B carrying *bla*$_{CMY-2}$ and *bla*$_{ADC-7}$ and *P. aeruginosa* 18SH strain, *bla*$_{PDC}$) was ceftazidime (CAZ) with increasing concentrations from 0.12 to 128 μg/mL. The antibiotic partner for the class A *bla*$_{CTX-M-9}$ strain was chosen to be cefepime (FEP) with variable concentration from 0.12 to 128 μg/mL. The addition of boronic acid inhibitors decreased the CAZ MIC for *E. coli* DH10B *bla*$_{ADC-7}$ from 16 to 2 μg/mL. When used against *E. coli* DH10B *bla*$_{CMY-2}$, the most potent inhibitors were **6s** and **6q**, decreasing the MICs for CAZ from 128 to 8 and 16 μg/mL, respectively. All of the other BATSIs decreased the CAZ MICs by 1- or 2-fold. The effect against *P. aeruginosa* clinical strain 18SH was minimal (only a 1-fold decrease with the addition of **6q, 6r,** or **6w**). When FEP was paired with **6q, 6s,** or **6x**, the *E. coli* DH10B *bla*$_{CTX-M-9}$ became susceptible to cefepime (FEP MICs decrease from 8 to 1 or 2 μg/mL). The other compounds lowered the FEP MICs by 1-fold.

Crystallographic Structures of ADC-7/Novel BATSI Complexes. To identify the structural basis for the observed inhibition of ADC-7 by these novel triazole boronic acids as well as to confirm the triazole functionality as a bioisostere for the R1 amide group found in the natural β-lactam substrates, X-ray crystal structures of five ADC-7/BATSI complexes were determined. Two compounds from Series **I** (Table 1, **6d** and **6e**), one compound from Series **II** (**6f**), the most effective inhibitor (**6q**), and one from Series **V** (**7r**) were selected for crystallographic analysis.

The ADC-7/BATSI complexes were determined to resolutions ranging from 1.80 to 2.04 Å (Table 4). In summary, all complexes crystallized in the $P2_1$ space group with four molecules in the asymmetric unit, as previously observed for

Table 4. Crystallographic Summary for ADC-7/Boronic Acid Complexes

	ADC-7/**6d**	ADC-7/**6e**	ADC-7/**6f**	ADC-7/**6q**	ADC-7/**6r**
cell constants (Å; deg)	$a = 89.62$	$a = 88.77$	$a = 88.55$	$a = 88.48$	$a = 88.93$
	$b = 80.78$	$b = 81.25$	$b = 81.46$	$b = 80.62$	$b = 81.10$
	$c = 107.00$	$c = 105.92$	$c = 105.67$	$c = 105.11$	$c = 105.94$
	$\beta = 112.47$	$\beta = 112.93$	$\beta = 113.10$	$\beta = 113.46$	$\beta = 113.06$
space group	$P2_1$	$P2_1$	$P2_1$	$P2_1$	$P2_1$
resolution (Å)	98.88–1.96 (1.964–1.957)[a]	97.55–1.82 (1.822–1.816)	97.20–2.04 (2.042–2.035)	50.00–1.80 (1.86–1.80)	81.82–1.74 (1.837–1.746)
unique reflections	96293 (988)	123054 (1239)	86979 (870)	125707 (12526)	116473 (5826)
R_{merge} (%)	5.0 (41.5)	5.4 (46.6)	7.2 (64.7)	9.0 (71.4)	8.6 (57.1)
R_{pim} (%)	2.9 (23.5)	3.1 (26.5)	4.3 (37.8)	4.9 (39.2)	5.6 (39.3)
CC(1/2)	0.999 (0.929)	0.998 (0.905)	0.995 (0.750)	0.940 (0.760)	0.995 (0.647)
completeness (%)	94.6 (98.9)	98.4 (98.8)	98.0 (98.6)	100.0 (100.0)	89.1 (50.0)
$\langle I/\sigma_I \rangle$	13.3 (2.0)	11.4 (1.9)	11.1 (2.1)	8.48 (2.6)	8.0 (1.5)
resolution range for refinement (Å)	98.88–1.96	97.55–1.82	97.19–2.04	44.26–1.80	81.95–1.74
number of protein residues	1424	1422	1422	1425	1423
number of water molecules	330	488	236	694	871
RMSD bond lengths (Å)	0.005	0.005	0.006	0.008	0.007
RMSD bond angles (deg)	1.38	1.30	1.53	1.51	1.52
R-factor (%)	21.9	22.0	22.1	19.4	21.6
R_{free} (%)[b]	25.1	25.6	25.4	23.8	27.3
average B-factor, protein atoms (Å^2)	44.77	47.41	46.86	35.54	40.68
average B-factor, inhibitor atom (Å^2)	58.36	66.93	48.98	58.3	54.82

[a]Values in parentheses are for the highest resolution shell. [b]R_{free} was calculated with 5% of reflections set aside randomly.

ADC-7/BATSI complexes.[8,10,11] The quality of the final models was evaluated with the wwPDB validation service[18] and showed that 96–98% of all residues were in the favorable region, with 2–4% in the allowed region, of the Ramachandran plots. The complexes with **6f**, **6q**, and **6r** were obtained by soaking ADC-7 crystals in inhibitor solutions, and the complexes with **6d** and **6e** were obtained through cocrystallization.

In each case, the initial $F_o − F_c$ electron density maps (contoured at 3σ) revealed unambiguous density that accounted for the presence of the inhibitor bound in the active site as well as covalent attachment to the catalytic Ser64. Inhibitors were built into the observed difference density, and the models were refined with Refmac5.[19] PDB-REDO was used to analyze and improve models between rounds of manual rebuilding in Coot.[20] $F_o − F_c$ omit maps were calculated for the final models (Figure 3) and confirmed the conformation of the inhibitor in the active site. In each complex, the four monomers were superposed, with RMSDs of all common Cα atoms ranging from 0.18 to 0.46 Å. The inhibitors within each complex bound in consistent conformations. For simplicity, the B monomer is used in figures and is representative of all monomers, although some differences are described in more detail below.

The boronic acid moiety interacts as expected with the enzyme in most of the complexes (Figure 4). The O1 hydroxyl group is observed to hydrogen bond with residues that comprise the oxyanion hole (main chain nitrogens of Ser64 and Ser315 and the main chain carbonyl oxygen of Ser315). However, in the complexes with **6e** and **6f** (Figure 4B,C), only the interactions with the main chain nitrogen of Ser64 and the main chain oxygen of Ser315 are observed. The O2 atom of the boronic acid is modified with a covalently bound phosphate ion, as has been observed in several other ADC-7/BATSI complexes where BATSI lacks an R2 group.[10] The triazole ring of each of the inhibitors is also observed to interact in a similar fashion in each

of the complexes. All complexes exhibited the expected hydrogen bonds between atoms N6 and N7 of the triazole ring and the side chain nitrogens of Gln120 and Asn152, albeit with some variations in the distances. Most were between 2.6 and 3.2 Å, although several were slightly longer (3.4–3.6 Å). Overall, these five structures confirm that, in ADC-7, the triazole is an effective amide bioisostere.

Specific Characteristics of the ADC-7/Series I Complexes. In each of the monomers of the ADC-7/**6d** and ADC-7/**6e** complexes (Figure 4C,B), the inhibitor is bound in the active site in similar conformations and follows a similar trajectory. The most variability is observed at the distal end of the inhibitors. In ADC-7/**6d** (Figure 4C), the linear trajectory of the inhibitor orients the benzoate group toward the lip of the active site, with the carboxylate group making a hydrogen bond with the main chain nitrogen of Ser317, via a water molecule, whereas in the ADC-7/**6e** complex (Figure 4B), the placement of the benzamide group is seen in two distinct conformations. In one (B and C monomers), the benzamide group is oriented toward Arg340, with the benzamide oxygen making a long hydrogen bond with this residue (3.2 Å). In the other (A and D monomers), the benzyl group is rotated ∼180° with the benzamide oriented away from Arg340.

Specific Characteristics of the ADC-7/Series II Complex. In the ADC-7/**6f** complex (Figure 4A), the inhibitor binds in the same conformation in all active sites of the four monomers. A thiophene replaces the aryl ring of Series I compounds at the distal end but does not make favorable interactions with the enzyme. Additionally, the shorter length of this inhibitor does not extend to the lip of the active site, where interactions with Ser317 were observed in the Series I complexes, and Arg340 is oriented toward the active site, likely due to the smaller sized inhibitor.
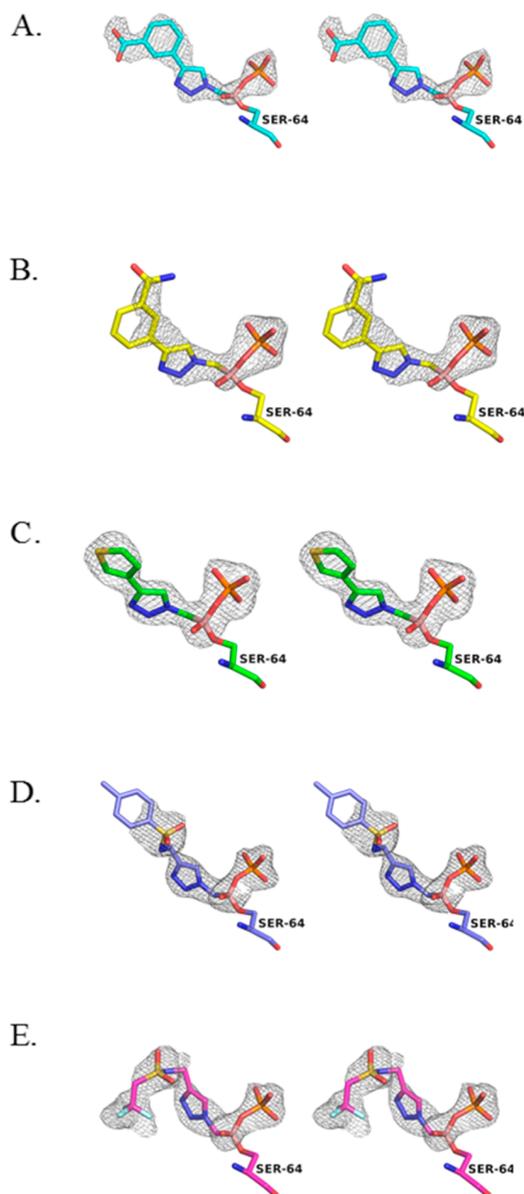
Figure 3. Stereoview of the $F_o - F_c$ omit maps for the ADC-7/BATSI complexes. (A) **6d**. (B) **6e**. (C) **6f**. (D) **6q**. (E) **6r**. This and all subsequent figures were made with PyMOL.[21] Omit maps are contoured at 3.0 σ and displayed as a gray cage surrounding the inhibitor. Carbon atoms are colored cyan for **6d**, yellow for **6e**, green for **6f**, purple for **6q**, and magenta for **6r**. Oxygen atoms, red; nitrogen, blue; boron atoms, pale pink; fluorine, pale cyan; phosphorus atoms, orange; sulfur, yellow.

Specific Characteristics of the ADC-7/Series IV Complex. Series **IV** explored more flexible groups that extend from the triazole ring. The sulfonamide linker (Figure 4D) displayed the best inhibition of all molecules tested from any of the series (K_i^{6q} 90 nM). Interestingly, the sulfonamide group itself does not make any favorable interactions with the enzyme. Arg340 is positioned out of the active site, with the distal tolyl group making favorable cation−π interactions with this residue. Distances from Arg340 to the centroid of the aryl ring range from 3.8 to 4.4 Å.

Specific Characteristics of the ADC-7/Series V Complex. To improve the binding affinity of **6q**, Series **V** molecules

Figure 4. Stereoview of the hydrogen bonding interactions in the ADC-7/BATSI complexes. (A) **6f**. (B) **6e**. (C) **6d**. (D) **6q**. (E) **6r**. Hydrogen bonding interactions are shown as dashed yellow lines and represent distances from 2.6 to 3.2 Å. Water molecules are shown as red spheres.

were designed. The structure of ADC-7 in complex with **6r** (Figure 4E), which replaces the tolyl group with a trifluoromethyl, was determined. The sulfonamide is oriented near Arg340 but is not within hydrogen bonding distance in monomers A and B, where Arg340 is swung out away from the active site. However, in monomers C and D, Arg340 adopts a

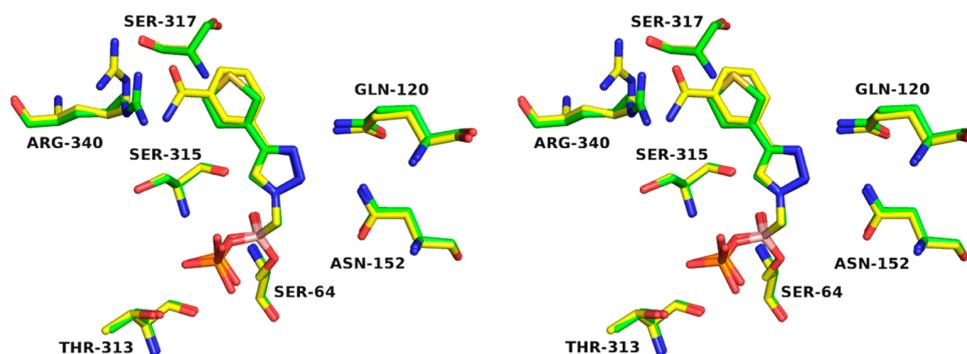**Figure 5.** Flexibility of Arg340 in inhibitor recognition. Superposition of ADC-7 in complex with **6f** (green) and **6e** (yellow).

344 conformation that positions it into the active site, and in these
345 instances, the sulfone interacts with this residue (2.5−2.9 Å).
346 The distal trifluoromethyl substituent is bent away from Arg340
347 and does not favorably interact with any residues in the active
348 site.

■ DISCUSSION AND CONCLUSION

350 This study explores the α-triazolylmethaneboronic acid scaffold
351 as a good template for ADC β-lactamase inhibition. Whereas
352 boronic acids have been identified as protease inhibitors since
353 the 1970s, only in the past decade has this class of compounds
354 been recognized as effective "bullets" in the antimicrobial
355 resistance arsenal.

356 α-Acylaminoboronic acids (Figure 1A) have been designed as
357 a good starting point to gain the proper interactions with the
358 enzyme. Indeed, several crystal structures of different β-
359 lactamase/α-amidomethaneboronic acid complexes point to
360 the presence of an amide binding site with specific enzyme
361 residues always interacting with the amide. In previous work on
362 ADC-7,[11] the triazole-containing compound **S06017** (Figure 1)
363 was synthesized, tested, and cocrystallized with the enzyme.

364 From the crystal structure, we observed that the triazole could
365 behave as a good amide bioisostere, with two lone pair nitrogens
366 able to interact with the canonical R$_1$ amide recognition residues
367 Asn152 and Gln120 that hydrogen bond with the two lone pairs
368 of the amide oxygen. Given the easy and mild access to the
369 triazole ring, with wide functional group tolerance, we wanted to
370 prove triazole is a good amide bioisostere and to improve the
371 activity of **S06017** (K_i 6.11 μM). Therefore, in this work, we
372 designed and synthesized 26 α-triazolylmethaneboronic acids,
373 differing the substituent at position 4 of the triazole. The K_i
374 values of these compounds vary from 90 nM to 38 μM, thus
375 confirming a good general affinity for the enzyme and a
376 consistent difference in activity due to insertion of varying
377 functional groups.

378 Compounds with a substituted phenyl ring directly attached
379 to the triazole (Series **I**, compounds **6a−e**) proved to be very
380 active with K_i values spanning from 200 nM to 1.61 μM. Two
381 compounds (**6d** and **6e**) from this series were crystallized in
382 complex with ADC-7: these complexes confirmed that the
383 triazole makes two of the three canonical interactions of the β-
384 lactam side chain, thus behaving as a good amide bioisostere.
385 Furthermore, from the crystal structure, the benzamide carbonyl
386 oxygen of the best inhibitor from this series, **6e** (K_i 200 nM),
387 makes a hydrogen bond with Arg340 (3.2 Å), suggesting the role
388 that interactions with Arg340 may play in increasing binding
389 affinity for these BATSIs. With **6d**, the carboxylate group of the
390 benzoate is flipped ∼180° from the benzamide, positioning the

391 negatively charged group away from Arg340. A favorable ionic
392 interaction might be expected between these groups in the other
393 conformation, but rotation of the benzoate results in a steric
394 clash between the two. Therefore, the carboxylate group is
395 instead oriented toward the solvent.

396 The replacement of the substituted phenyl ring with an
397 electron rich (i.e., the thiophene in **6f**) or electron poor (the
398 pyridine and pyrazine in **6g** and **6h**, respectively) heterocycle
399 maintain a similar level of activity (K_i's from 1 to 5.3 μM). From
400 this Series **II**, the structure of the enzyme in complex with
401 compound **6f** was superposed with the ADC-7/**6e** complex
402 (Figure 5). The two compounds have a 5-fold difference in
403 activity (K_i of 1 μM for **6f** vs 200 nM for **6e**): indeed, the
404 thiophene ring is placed in the same position as the phenyl ring
405 from Series **I** and does not take advantage of any specific
406 interaction with the enzyme. The most distinctive difference
407 between the two structures is the positioning of Arg340, a
408 residue which exhibits flexibility: ADC-7/**6f** shows Arg340
409 oriented toward the active site in the presence of the smaller
410 thiophene inhibitor. In contrast, the ADC-7/**6e** complex
411 (yellow) shows Arg340 oriented away from the active site to
412 accommodate the binding of a larger inhibitor and to be
413 positioned at a proper distance for hydrogen bonding.

414 In an attempt to gain interactions with Arg340, Series **III** and
415 **IV** were synthesized to elongate the substituent on the triazole.
416 The addition of a substituted phenyloxymethyl linker as in Series
417 **III** (compounds **6i−l**) did not significantly improve activity (K_i's
418 from 0.98 to 2.84 μM), whereas the substituted aminomethyl
419 bridge exploited the most significant differences. In Series **IV**,
420 activity in fact dramatically dropped when a protonated
421 aminomethyl (compound **6m**) or acylamino side chain
422 (compounds **6n** and **6p**) was introduced (K_i's from 8.7 to
423 33.8 μM). In contrast, compound **6q** with a *p*-tolylsulfonylami-
424 no substituent displayed the best activity among the α-triazolyl
425 BATSIs (K_i 90 nM), pointing to **6q** as one of the best achiral
426 inhibitors of class C β-lactamases. The analysis of the ADC-7/**6q**
427 complex revealed how the tetrahedral geometry of the
428 sulfonamide, as in **6q**, allows for cation−π interactions with
429 Arg340 (Figure 6), which is probably not reached when a planar
430 geometry is introduced through an amide linker as in **6p**.

431 Notably, the structure of **6q** does not resemble the natural
432 substrate of the β-lactamase but displays a pronounced
433 inhibition activity. In fact, when compared to α-acylaminome-
434 thaneboronic acids previously synthesized[22] (Figure 7),
435 compound **6q** (K_i 90 nM) is 3 times more active than the
436 boronic acid bearing the ceftazidime side chain (K_i 310 nM) and
437 almost 9 times more active than the cephalothin analog (K_i 780
438 nM). The activity of the α-triazolylboronic acid is significantly
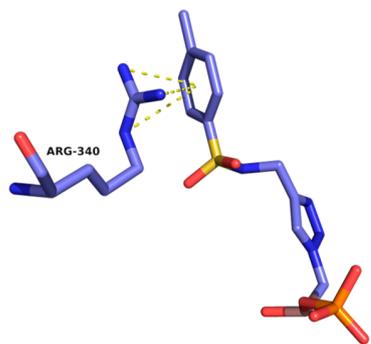
Figure 6. Cation−π interactions between Arg340 and the aryl ring of **6q**, the BATSI with the highest affinity to ADC-7. Interactions, indicated by dashed yellow lines, are drawn from Arg340 to the centroid of the aryl ring, with distances ranging from 3.8 to 4.4 Å.

less compared to the one of the α-sulfonylaminomethaneboronic acids bearing a distal tetrazole in the side chain (compound **CR192**). From the structural analysis of such derivatives, it became evident how the increase in activity was due to the interaction of the negatively charged tetrazole with a distal binding site formed by Asn213 and Ser317.

Given the length and trajectory of **6q**, the distal functional groups of this molecule do not extend to the outer edge of the active site where Asn213 is located. However, the Cβ atom of Ser317 is within the van der Waals distance of the aryl ring of **6q** (~4.3−4.5 Å), thus giving the opportunity for further optimizing the molecule. A validation of the α-triazolylmethaneboronic structure of **6q** as a template for further derivatization was obtained through microbiological assays in *E. coli* expressing ADC-7 of compounds **6a−p**. All compounds lowered the MIC (16 μg/mL) of CAZ from 1- to 4-fold, and the MIC values were in good agreement with K_i's (Chart 1), thus confirming a good permeability of these compounds.

In an attempt to improve **6q** activity and eventually reach the distal binding site of ADC-7, we obtained an additional nine compounds (Figure 2, Series **V**, compounds **6r−z**). Unfortunately, none of the compounds of Series **V** improve activity toward ADC-7 with K_i's spanning from 0.21 to 1.46 μM (Table 3). Compound **6r** was crystallized in complex with ADC-7. In **6r**, the tolyl group of **6q** is replaced with a trifluoroethyl group, which is unable to make the cation−π interaction seen in the ADC-7/**6q** complex: Arg340 in fact points away, likely resulting in lower binding affinity of the compound. Compounds **6t−x** all contain a methylene linker that may extend the distal group away from Arg340 and prevent this interaction, resulting in lower binding affinities as well. Compounds **6y** and **6z** more closely resemble **6q** and **6r** as they lack the flexible methylene linker. Compound **6y** contains a cyano group as compared to the

tetrazole of **6z**, which might impact the ability of the aryl rings to form cation−π interactions with Arg340. Overall, the lower binding affinities of Series **V** might point to the inability of reaching the distal binding site (Arg213 and Ser317) and at the same time to the loss of interaction with Arg340, which is a residue that is unique to the ADC enzymes as compared to other class C β-lactamases. Known to be a contributor to protein− protein and protein−ligand interactions, the cation−π interaction observed in these ADC-7/inhibitor complexes suggests that it is important for the design of future series. Arg340 may be a key residue to target as it is unique to this class of enzymes and has shown the ability to interact with a variety of different functional groups (amide, carboxylate, trifluoromethyl, phenyl) in a variety of different interactions, such as Coulombic, ionic, hydrogen bond, and cation−π. In addition, the flexibility shown by Arg340 allows ADC-7 to accommodate BATSIs with larger R1 groups that are able to reach the residues at the lip of the active site (such as Asn213 and Ser317).

In summary, when the highly efficient and versatile synthetic method known as click chemistry is employed, a new class of β-lactamases inhibitors has been synthesized, starting from the easily accessible pinanediol and azidomethaneboronate. All 26 BATSIs displayed K_i values spanning from low micromolar to nanomolar values, with compound **6q** being among the best achiral inhibitors of the class C β-lactamases. Five of these inhibitors were crystallized in complex with ADC-7 revealing that, besides the interaction of the boronic moiety with the catalytic serine residue, the triazole is able to maintain the typical interactions of the extensively explored and parent amidomethaneboronic inhibitors, thus acting as a good amide bioisostere. Finally, this new class of inhibitors proved to be able to restore CAZ and FEP activity against class C and A β-lactamase strains.

■ METHODS

Synthesis. Reactions were monitored by thin layer chromatography (TLC), which were visualized by UV fluorescence and by Hanessian's cerium molybdate stain. Deoxygenated water was obtained through sonication. Chromatographic purification of the compounds was performed on silica gel (particle size 0.05−0.20 mm). Melting points were measured in open capillary tubes on a Stuart SMP30 Melting Point apparatus. Optical rotations were determined at 20 °C on a PerkinElmer 241 polarimeter and are expressed in 10^{-1} deg cm^2 g^{-1}. ^{1}H and ^{13}C NMR spectra were recorded on a Bruker Avance-400 MHz spectrometer. Chemical shifts (δ) are reported in ppm and were calibrated to the residual signals of the deuterated solvent.[21] Multiplicity is given as s = singlet, d = doublet, t = triplet, q = quartet, m = multiplet, and br = broad signal; coupling constants (J) are given in Hz. Two-dimensional NMR techniques (COSY, HMBC, HSQC) were used to aid in the assignment of signals in ^{1}H and ^{13}C spectra. Particularly, in

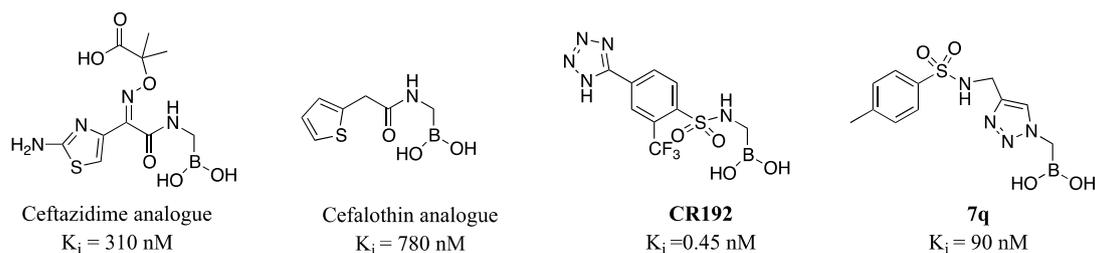| Ceftazidime analogue	Cefalothin analogue	**CR192**	**7q**
K_i = 310 nM	K_i = 780 nM	K_i =0.45 nM	K_i = 90 nM

Figure 7. Structures and K_i values of previously synthesized α-acylaminoboronic acids.

H

the ^{13}C spectra, the signal of the boron-bearing carbon atom, which tends to be broadened, and the signal of the quaternary triazole carbon are often beyond the detection limit, but their resonances were unambiguously determined by HSQC and HMBC; melting points of free boronic acids **6b−z** were not reproducible due to dehydration.[23] Mass spectra were determined on an Agilent Technologies LC-MS (n) Ion Trap 6310A (ESI, 70 eV). High-resolution mass spectra were recorded on an Agilent Technologies 6520 Accurate-Mass Q-TOF LC/MS.

The purity of all tested compounds was above 95%, determined by analytical HPLC-MS (see the Supporting Information for a detailed description). Synthesis and characterization of compounds **2, 3, 4b−e, 4g−h, 4j−w, 4y, 5b−e, 5g−h, 5j−w, 5y, 5z, 6b−e, 6g−h,** and **6j−z** are reported in the Supporting Information.

Microbiology. MICs were performed as previously described[7] and according to Clinical and Laboratory Standards Institute (CLSI) guidelines,[25] using a 6×10^4 cfu/mL inoculum. Bacterial cultures were grown overnight in Mueller-Hinton (MH) broth supplemented with 20 μg/mL chloramphenicol. We employed the *E. coli* construct that was previously validated as a representative of ADC-7 in a uniform genetic background (bla_{ADC-7} was directionally cloned in pBC SK (−) phagemid vector). Bacterial liquid culture was diluted using MH broth to a 6×10^4 cfu/mL final concentration, and the antibiotic partner, CAZ or FEP, was added at concentrations from 128 to 0.06 μg/mL. BATSIs were constant at 4 μg/mL. The plates were incubated at 37 °C overnight, and the results were recorded the next day.

Purification and Kinetics. ADC-7 β-lactamase was expressed as previously described[9] and purified using cation exchange chromatography. For the purification of ADC-7, cell pellets were suspended in 25 mM 3-(N-morpholino) propane-sulfonic acid (MOPS buffer), pH 6.5, with 1× HALT protease inhibitor cocktail (Sigma) and DNase I (50 Units). The solution was sonicated for 4×30 s intervals on ice. The lysate was centrifuged at 15 000 rpm at 4 °C for 20 min. The cell-free extract was then loaded onto a carboxymethyl-cellulose column by gravity flow at 4 °C (5 mL resin per gram of cell pellet). The column was washed with 100 mL of 25 mM MOPS, pH 6.5, at a flow rate of 0.3 mL/min followed by elution with a linear gradient of 0−0.5 M NaCl in 25 mM MOPS, pH 6.5. The fractions containing ADC-7 were collected, pooled, and then dialyzed in 2×5 L of 25 mM MOPS, pH 6.5 at 4 °C. The dialyzed ADC-7 was concentrated to at least 10 mg/mL using an Amicon Ultra centrifugal filter unit with Ultra-10 membrane (Millipore). The concentration of ADC-7 was determined using the A_{280} with an extinction coefficient of 46 300 $M^{-1}cm^{-1}$, as calculated for the expressed residues D24-K383 of ADC-7 by the ProtParam tool on the ExPASy bioinformatics portal.[24]

The inhibition constants (K_i) for each of the BATSIs with ADC-7 were determined using competition kinetics. When nitrocefin (NCF) was utilized as a colorimetric substrate of ADC-7, boronic acids **7a−q** were tested as inhibitors of ADC-7 β-lactamase as previously described.[7,9,10] The measurements of the initial velocities were performed with the addition of 100 μM NCF after a 5 min preincubation of the enzyme (2 nM) with increasing concentration of the inhibitor. To determine the average velocities (v_0), data from three experiments were fit to the equation:

$$\nu_0 = \nu_u - \left\{ \frac{\nu_u [I]}{IC_{50} + [I]} \right\}$$

where ν_u represents the NCF uninhibited velocity and IC_{50} represents the inhibitor concentration that results in a 50% reduction of ν_u. The K_i values for all 26 BATSIs were corrected for the NCF affinity ($K_m = 20$ μM) with the Cheng-Prusoff[30] equation:

$$K_i = IC_{50} \Big/ \left(1 + \frac{[NCF]}{K_{mNCF}} \right)$$

The data analysis was performed using EnzFitter and Origin 2019b.

Crystallization and Structure Determination. Structures of ADC-7 in complexes with the inhibitors were obtained via both soaking and cocrystallization methods. For soaks, ADC-7 crystals were grown via hanging drop vapor diffusion at room temperature as previously described.[11] Preformed crystals were harvested using a nylon loop and soaked in crystallization buffer containing the BATSI at concentrations ranging from 2 to 16 mM for between 5 and 25 min. Co-crystals were grown in 0.1 M succinate/phosphate/glycine (SPG buffer), pH 5.0, 25% w/v PEG-1500, with 3.5−3.75 mg/mL ADC-7 and 1 mM BATSIs in the initial crystallization buffer.

Data for each of the complexes were measured from single crystals at the Advanced Photon Source at Argonne National Laboratory (LS-CAT sector). All diffraction images were processed with XDS[25] with the exception of the ADC-7/**6q** data set, where HKL2000[26] was used. For the ADC-7/**6r** data set, additional processing of the structure factors was performed using STARANISO.[27] Structures were determined by molecular replacement with Phaser,[28] using the ADC-7/S02030 complex (PDB 4U0X), with water, ion, and inhibitor atoms removed, as the starting model. Refinement of the models was done with Refmac5 in the CCP4 suite,[29] and model building was done with Coot.[20b] The coordinates and structure factors for the ADC-7/BATSI complexes were deposited in the Protein Data Bank with the following codes: 6TZF (**6d**), 6TZG (**6e**), 6TZH (**6f**), 6TZI (**6r**), and 6TZJ (**6q**).

■ ASSOCIATED CONTENT

Ⓢ Supporting Information

The Supporting Information is available free of charge at https://pubs.acs.org/doi/10.1021/acsinfecdis.0c00254.

> Synthesis and characterization of compounds **2, 3, 4a−z, 5b−z,** and **6b−z**; a statement of purity of compounds **6b−z**; copies of ^1H and ^{13}C NMR spectra of compounds **6b−z** (PDF)

■ AUTHOR INFORMATION

Corresponding Authors

Fabio Prati − *Department of Life Sciences, University of Modena and Reggio Emilia, Modena 41125, Italy;* ⓘ orcid.org/0000-0002-0650-9540; Phone: (+39)059-2055056; Email: fabio.prati@unimore.it

Robert A. Bonomo − *Louis Stokes Cleveland Department of Veterans Affairs Medical Center, Research Service, Cleveland, Ohio 44106, United States; Departments of Medicine, Pharmacology, Biochemistry and Molecular Biology and Microbiology, Case Western Reserve University, Cleveland, Ohio 44106, United States; CWRU-Cleveland VAMC Center for*

636   *Antimicrobial Resistance and Epidemiology (Case VA CARES),*
637   *Cleveland, Ohio 44106, United States;* ⊙ orcid.org/0000-
638   0002-3299-894X; Phone: (+1) 216 791 3800;
639   Email: robert.bonomo@va.gov

640 **Bradley J. Wallar** − *Department of Chemistry, Grand Valley State*
641   *University, Allendale, Michigan 49401, United States;*
642   Phone: (+1) 616-331-5879; Email: wallarb@gvsu.edu

643 **Authors**

644   **Emilia Caselli** − *Department of Life Sciences, University of*
645   *Modena and Reggio Emilia, Modena 41125, Italy;* ⊙ orcid.org/
646   0000-0002-7248-9453

647   **Francesco Fini** − *Department of Life Sciences, University of*
648   *Modena and Reggio Emilia, Modena 41125, Italy;* ⊙ orcid.org/
649   0000-0003-2555-9313

650   **Maria Luisa Introvigne** − *Department of Life Sciences and*
651   *Clinical and Experimental Medicine PhD Program, University of*
652   *Modena and Reggio Emilia, Modena 41125, Italy*

653   **Mattia Stucchi** − *Department of Life Sciences, University of*
654   *Modena and Reggio Emilia, Modena 41125, Italy*

655   **Magdalena A. Taracila** − *Louis Stokes Cleveland Department of*
656   *Veterans Affairs Medical Center, Research Service, Cleveland,*
657   *Ohio 44106, United States; Department of Medicine, Case*
658   *Western Reserve University, Cleveland, Ohio 44106, United*
659   *States*

660   **Erin R. Fish** − *Department of Chemistry, Grand Valley State*
661   *University, Allendale, Michigan 49401, United States*

662   **Kali A. Smolen** − *Department of Chemistry, Grand Valley State*
663   *University, Allendale, Michigan 49401, United States*

664   **Philip N. Rather** − *Department of Microbiology & Immunology,*
665   *Emory University School of Medicine, Atlanta, Georgia 30322,*
666   *United States*

667   **Rachel A. Powers** − *Department of Chemistry, Grand Valley*
668   *State University, Allendale, Michigan 49401, United States;*
669   ⊙ orcid.org/0000-0002-9968-8284

670 Complete contact information is available at:
671 https://pubs.acs.org/10.1021/acsinfecdis.0c00254

672 **Author Contributions**

673 E.C., M.S., M.L.I., F.F., and F.P. synthesized and characterized
674 all of the BATSI compounds. M.A.T. and R.A.B. performed
675 microbiological assays and kinetics. R.A.P., B.J.W., E.R.F., and
676 K.A.S. determined all of the crystal structures. E.C. wrote the
677 first draft of the manuscript; all authors have contributed and
678 have given approval to the final version of the manuscript.

679 **Notes**

680 The authors declare no competing financial interest.

710 ■ **ABBREVIATIONS**

711 BATSI, boronic acid transition state inhibitors; ADC,
712 *Acinetobacter* derived cephalosporinase; MICs, minimum
713 inhibitory concentrations; CAZ, ceftazidime; FEP, cefepime;
714 HSQC, heteronuclear single-quantum coherence; HMBC,
715 heteronuclear multiple-bond correlation; LC/MS, liquid
716 chromatography/mass spectrometry; CuAAC, copper-catalyzed
717 alkyne azide cycloaddition; *t*-BuOH, *tert*-butanol

718 ■ **REFERENCES**

719 (1) Zhen, X., Stalsby Lundborg, C., Sun, X., Hu, X., and Dong, H.
720 (2019) Economic burden of antibiotic resistance in ESKAPE
721 organisms: a systematic review. *Antimicrobial Resistance and Infection*
722 *Control 8*, 137.
723 (2) Tacconelli, E., Carrara, E., Savoldi, A., Harbarth, S., Mendelson,
724 M., Monnet, D. L., Pulcini, C., Kahlmeter, G., Kluytmans, J., Carmeli,
725 Y., Ouellette, M., Outterson, K., Patel, J., Cavaleri, M., Cox, E. M.,
726 Houchens, C. R., Grayson, M. L., Hansen, P., Singh, N.,
727 Theuretzbacher, U., Magrini, N., et al. (2018) Discovery, research,
728 and development of new antibiotics: the WHO priority list of
729 antibiotic-resistant bacteria and tuberculosis. *Lancet Infect. Dis. 18*,
730 318−327.
731 (3) Wong, D., Nielsen, T. B., Bonomo, R. A., Pantapalangkoor, P.,
732 Luna, B., and Spellberg, B. (2017) Clinical and Pathophysiological
733 Overview of Acinetobacter Infections: a Century of Challenges. *Clin.*
734 *Microbiol. Rev. 30*, 409−447.
735 (4) Isler, B., Doi, Y., Bonomo, R. A., and Peterson, D. L. (2019) New
736 Treatment Options against Carbapenem-Resistant *Acinetobacter*
737 *baumannii* Infections. *Antimicrob. Agents Chemother. 63*, e01110−18.
738 (5) Mosley, J. F., Smith, L. L., Parke, C. K., Brown, J. A., Wilson, A. L.,
739 and Gibbs, L. V. (2016) Ceftazidime-Avibactam (Avycaz): For the
740 Treatment of Complicated Intra-Abdominal and Urinary Tract
741 Infections. *Pharmacy and Therapeutics 41*, 479−483.
742 (6) Griffith, D. C., Sabet, M., Tarazi, Z., Lomovskaya, O., and Dudley,
743 M. N. (2019) Pharmacokinetics/Pharmacodynamics of Vaborbactam,
744 a Novel Beta-Lactamase Inhibitor, in Combination with Meropenem.
745 *Antimicrob. Agents Chemother. 63*, e01659-18.
746 (7) Wong, D., and van Duin, D. (2017) Novel Beta-Lactamase
747 inhibitors: Unlocking Their Potential in Therapy. *Drugs 77*, 615−628.
748 (8) Caselli, E., Romagnoli, C., Powers, R. A., Taracila, M. A., Bouza, A.
749 A., Swanson, H. C., Smolen, K. A., Fini, F., Wallar, B. J., Bonomo, R. A.,
750 and Prati, F. (2018) Inhibition of Acinetobacter-Derived Cephalospor-
751 inase: Exploring the Carboxylate Recognition Site Using Novel *β*-
752 Lactamase Inhibitors. *ACS Infect. Dis. 4*, 337−348.
753 (9) Crompton, I. E., Cuthbert, B. K., Lowe, G., and Waley, S. G.
754 (1988) *β*-lactamase inhibitors. The inhibition of serine *β*-lactamases by
755 specific boronic acids. *Biochem. J. 251*, 453−459.
756 (10) Powers, R. A., Swanson, H. C., Taracila, M. A., Florek, N. W.,
757 Romagnoli, C., Caselli, E., Prati, F., Bonomo, R. A., and Wallar, B. J.
758 (2014) Biochemical and Structural Analysis of Inhibitors Targeting the

ADC-7 Cephaloporinases of Acinetobacter Baumanii. *Biochemistry 53*, 7670−7679.

(11) Bouza, A. A., Swanson, H. C., Smolen, K. A., VanDine, A. L., Taracila, M. A., Romagnoli, C., Caselli, E., Prati, F., Bonomo, R. A., Powers, R. A., and Wallar, B. J. (2018) Structure-Based Analysis of Boronic Acids as Inhibitors of *Acinetobacter*-Derived Cephalosporinase-7, a Unique Class C *β*-Lactamase. *ACS Infect. Dis. 4*, 325−336.

(12) (a) Li, H., Aneja, R., and Chaiken, I. (2013) *Molecules 18*, 9797−9817. (b) Tron, G. C., Pirali, T., Billington, R. A., Canonico, P. L., Sorba, G., and Genazzani, A. A. (2008) *Med. Res. Rev. 28*, 278−308. (c) Hou, J., Liu, X., Shen, J., Zhao, G., and Wang, P. G. (2012) *Expert Opin. Drug Discovery 7*, 489−501. (d) Lauria, A., Delisi, R., Mingoia, F., Terenzi, A., Martorana, A., Barone, G., and Almerico, A. M. (2014) *Eur. J. Org. Chem. 2014*, 3289−3306. (e) Bonandi, E., Christodoulou, M. S., Fumagalli, G., Perdicchia, D., Rastelli, G., and Passarella, D. (2017) The 1,2,3-triazole ring as bioisostere in medicinal chemistry. *Drug Discovery Today 22*, 1572−1581.

(13) (a) Meldal, M., and Tornøe, C. W. (2008) Cu-catalyzed azide-alkyne cycloaddition. *Chem. Rev. 108*, 2952−3015. (b) Rostovtsev, V. V., Green, L. G., Fokin, V. V., and Sharpless, K. B. (2002) A stepwise Huisgen cycloaddition process: copper(I)-catalyzed regioselective ligation of azides and terminal alkynes. *Angew. Chem., Int. Ed. 41*, 2596−2599.

(14) (a) Caselli, E., Romagnoli, C., Vahabi, R., Taracila, M. A., Bonomo, R. A., and Prati, F. (2015) Click Chemistry in Lead Optimization of Boronic Acids as *β*-Lactamase Inhibitors. *J. Med. Chem. 58*, 5445−58. (b) Romagnoli, C., Caselli, E., and Prati, F. (2015) Synthesis of 1,2,3-triazol-1-yl-methaneboronic acids via click chemistry: an easy access to a new potential scaffold for protease inhibitors. *Eur. J. Org. Chem. 2015*, 1075−1083.

(15) Molander, G. A., Cavalcanti, L. N., Canturk, B., Pan, P.-S., and Kennedy, L. E. (2009) Efficient Hydrolysis of Organotrifluoroborates via Silica Gel and Water. *J. Org. Chem. 74*, 7364−7369.

(16) Kabalka, G. W., and Coltuclu, V. (2009) Thermal and Microwave Hydrolysis of Organotrifluoroborates Mediated by Alumina. *Tetrahedron Lett. 50*, 6271−6272.

(17) Yuen, A. K. L., and Hutton, C. A. (2005) Deprotection of Pinacolyl Boronate Esters via Hydrolysis of Intermediate Potassium Trifluoroborates. *Tetrahedron Lett. 46*, 7899−7903.

(18) Berman, H., Henrick, K., and Nakamura, H. (2003) Announcing the worldwide Protein Data Bank. *Nat. Struct. Mol. Biol. 10*, 980.

(19) Murshudov, G. N., Vagin, A. A., and Dodson, E. J. (1997) Refinement of macromolecular structures by the maximum-likelihood method. *Acta Crystallogr., Sect. D: Biol. Crystallogr. 53*, 240−255.

(20) (a) Joosten, R. P., Long, F., Murshudov, G. N., and Perrakis, A. (2014) The PDB_REDO server for macromolecular structure model optimization. *IUCrJ 1* (Pt 4), 213−220. (b) Emsley, P., and Cowtan, K. (2004) Coot: Model-building tools for molecular graphics. *Acta Crystallogr., Sect. D: Biol. Crystallogr. 60*, 2126−2132.

(21) (2010) *The PyMOL Molecular Graphics System*, Version 1.3, Schrodinger, LLC, New York.

(22) Drawz, S. M., Babic, M., Bethel, C. R., Taracila, M., Distler, A. M., Ori, C., Caselli, E., Prati, F., and Bonomo, R. A. (2010) Inhibition of the class C beta-lactamase from *Acinetobacter* spp.: insights into effective inhibitor design. *Biochemistry 49*, 329−40.

(23) Hall, D. G., Ed. (2005) *Boronic Acids*, Wiley-VCH.

(24) Gasteiger, E., Hoogland, C., Gattiker, A., Duvaud, S., Wilkins, M. R., Appel, R. D., and Bairoch, A. (2005) Protein Identification and Analysis Tools on the ExPASy Server. In *The Proteomics Protocols Handbook* (Walker, J. M., Ed.), pp 571−607, Humana Press.

(25) Kabsch, W. (2010) *Acta Crystallogr., Sect. D: Biol. Crystallogr. 66*, 125−132.

(26) Otwinowski, Z., and Minor, W. (1997) *Methods Enzymol. 276*, 307−326.

(27) Tickle, I. J., Flensburg, C., Keller, P., Paciorek, W., Sharff, A., Vonrhein, C., and Bricogne, G. (2018) *STARANISO*, Global Phasing Ltd., Cambridge, United Kingdom (http://staraniso.globalphasing.org/cgi-bin/staraniso.cgi).

(28) McCoy, A. J., Grosse-Kunstleve, R. W., Adams, P. D., Winn, M. D., Storoni, L. C., and Read, R. J. (2007) Phaser crystallographic software. *J. Appl. Crystallogr. 40*, 658−674.

(29) Murshudov, G. N., Vagin, A. A., and Dodson, E. J. (1997) Refinement of macromolecular structures by the maximum-likelihood method. *Acta Crystallogr., Sect. D: Biol. Crystallogr. 53*, 240−255.

(30) Cheng, Y.-C., and Prusoff, W. H. (1973) Relationship between the inhibition constant (K_I) and the concentration of inhibitor which causes 50% inhibition (I_{50}) of an enzymatic reaction. *Biochem. Pharmacol. 22* (23), 3099−3108.

K